ISSN 1674-1056
http://cpb.iphy.ac.cn
http://iopscience.iop.org/cpb
中国物理 B
Chinese Physics
中国物理
Chinese Physics B

Flexible broadband polarization converter based on metasurface at microwave band

Qi Wang(王奇), Xiangkun Kong(孔祥鲲), Xiangxi Yan(严祥熙), Yan Xu(徐岩), Shaobin Liu(刘少斌), Jinjun Mo(莫锦军), Xiaochun Liu(刘晓春)

Citation: Chin. Phys. B . 2019, 28(7): 074205. **doi:** 10.1088/1674-1056/28/7/074205
Journal homepage: http://cpb.iphy.ac.cn; http://iopscience.iop.org/cpb

What follows is a list of articles you may be interested in

Pressure dependent modulation instability in photonic crystal fiber filled with argon gas

He-Lin Wang(王河林), Ai-Jun Yang(杨爱军), XiaoLong Wang(王肖隆), Bin Wu(吴彬), Yi Ruan(阮义)
Chin. Phys. B . 2018, 27(9): 094221. **doi:** 10.1088/1674-1056/27/9/094221

Wideband linear-to-circular polarization conversion realized by a transmissive anisotropic metasurface

Bao-Qin Lin(林宝勤), Jian-Xin Guo(郭建新), Bai-Gang Huang(黄百钢), Lin-Bo Fang(方林波), Peng Chu(储鹏), Xiang-Wen Liu(刘湘雯)
Chin. Phys. B . 2018, 27(5): 054204. **doi:** 10.1088/1674-1056/27/5/054204

Double-rod metasurface for mid-infrared polarization conversion

Yang Pu(蒲洋), Yi Luo(罗意), Lu Liu(刘路), De He(何德), Hongyan Xu(徐洪艳), Hongwei Jing(景洪伟), Yadong Jiang(蒋亚东), Zhijun Liu(刘志军)
Chin. Phys. B . 2018, 27(2): 024202. **doi:** 10.1088/1674-1056/27/2/024202

A linear-to-circular polarization converter based on I-shapedcircular frequency selective surfaces

Jia-Liang Wu(吴家梁), Bao-Qin Lin(林宝勤), Xin-Yu Da(达新宇), Kai Wu(吴凯)
Chin. Phys. B . 2017, 26(9): 094201. **doi:** 10.1088/1674-1056/26/9/094201

Wide-angle and broadband graded-refractive-index antireflection coatings

Zhang Jun-Chao, Xiong Li-Min, Fang Ming, He Hong-Bo
Chin. Phys. B . 2013, 22(4): 044201. **doi:** 10.1088/1674-1056/22/4/044201

Flexible broadband polarization converter based on metasurface at microwave band*

Qi Wang(王奇)[1], Xiangkun Kong(孔祥鲲)[1,†], Xiangxi Yan(严祥熙)[1], Yan Xu(徐岩)[1], Shaobin Liu(刘少斌)[1], Jinjun Mo(莫锦军)[2], and Xiaochun Liu(刘晓春)[3]

[1] *Key Laboratory of Radar Imaging and Microwave Photonics, Ministry of Education, College of Electronic and Information Engineering, Nanjing University of Aeronautics and Astronautics, Nanjing* 211106, *China*

[2] *School of Aeronautics and Astronautics, Central South University, Changsha* 410083, *China*

[3] *Research Institute for Special Structures of Aeronautical Composite Aviation Industry Corporation of China, Aeronautical Science Key Laboratory for High Performance Electromagnetic Windows, Jinan* 250000, *China*

(Received 4 March 2019; revised manuscript received 6 April 2019; published online 30 May 2019)

A flexible broadband linear polarization converter is proposed based on the metasurface operating at microwave band. To achieve bandwidth extension property, long and short metallic arc wires, as well as the metallic disks placed over a ground plane, are combined into the polarizer, which can generate three neighboring resonances. Due to the combination of the first two resonances and the optimized size and thickness of the unit cell, the polarization converter can have a weak incident angle dependence. Both simulated and measured results confirm that the average polarization conversion ratio is over 85% from 11.3 GHz to 20.2 GHz within a broad range of incident angle from 0° to 45°. Moreover, the proposed polarization converter based on flexible substrates can be applied for conformal design. The simulation and experiment results demonstrate that our designed polarizer still keeps high polarization conversion efficiency, even when it adheres to convex cylindrical surfaces. The periodic metallic structure of the designed polarizer has great potential application values in the microwave, terahertz, and optic regimes.

Keywords: polarization converter, flexible metasurface, wide-angle, broadband

PACS: 42.25.Bs, 42.25.Ja, 78.67.Pt, 92.60.Ta **DOI:** 10.1088/1674-1056/28/7/074205

1. Introduction

Polarization is an important characteristic of electromagnetic (EM) wave, and fully manipulating the polarization state is highly desirable in several electromagnetic applications.[1,2] Metamaterials, which have extraordinary electromagnetic properties that natural materials do not have,[3,4] provide a very effective way to manipulate several basic properties of the EM wave and can be applied to polarizers,[5–7] lenses,[8,9] high gain antennas,[10,11] and invisible cloaks.[12,13] Compared with the conventional polarizers using the Faraday effect[14] and twisted nematic liquid crystal, the polarization converters based on the metamaterials are relatively thin (subwavelength thickness) and light. On the basis of metamaterial technology, many studies have been devoted to controlling the polarization state of EM waves recently. Many polarization converters based on anisotropic and chiral metamaterials have been proposed.[15–17] However, these polarizers suffer from narrow bandwidth, which extremely limits their practical applications. To expand the bandwidth, stacked multilayer structures,[18–24] gold helix structures,[25] and anisotropic high-impedance surfaces[26] can be utilized. However, these polarizers are hard to fabricate and integrate into the existing systems due to their complex structures or unacceptable thickness. Planar polarizers based on metasurfaces that are ultra-thin layered two-dimension metamaterials[27–35] were designed to achieve both wideband bandwidth and higher conversion efficiency. Nevertheless, these proposed polarization devices may not keep high polarization efficiency within a broad range of incident angles. Thus, polarization devices with high polarization efficiency, wideband, and high angular tolerance are highly desirable.

Rendering flexibility to metamaterials can make it possible to adhere flexible devices to all surfaces or wrap transparent and light metamaterials around objects, from which many terahertz and microwave applications[36–45] can significantly benefit. Kamali *et al.*[39] showed that cylindrical lenses covered with metasurfaces could be used as aspherical lenses to focus light onto a point by using a flexible substrate. Youn *et al.*[45] proposed and demonstrated an optically transparent and flexible microwave absorber that provided a method to use a three-dimensional (3D) design. Therefore, flexible metamaterials open up a whole new range of practical applications. Additionally, to the best of our knowledge, there is a lack of polarizer based on flexible metamaterials or metasurfaces at microwave bands.

In this paper, we design a reflective broadband linear po-

*Project supported by the Fundamental Research Funds for the Central Universities, China (Grant No. kfjj20180401), the National Natural Science Foundation of China (Grant No. 61471368), the Aeronautical Science Foundation of China (Grant No. 20161852016), the China Postdoctoral Science Foundation (Grant No. 2016M601802), and Jiangsu Planned Projects for Postdoctoral Research Funds, China (Grant No. 1601009B).

†Corresponding author. E-mail: xkkong@nuaa.edu.cn

© 2019 Chinese Physical Society and IOP Publishing Ltd

larizer composed of metallic disks and asymmetric arc metallic wires placed over flexible substrates. The long arc metallic wire resonator provides the main resonances. The short arc metallic wire and the metallic disk work as couplers to adjust the resonance frequencies and intensities. Both simulated and experimental results have demonstrated that the designed polarizer has a wide operating bandwidth from 11.3 GHz to 20.2 GHz under normal incidence of both *x*- and *y*-polarized waves. It can also keep high-efficient polarization conversion when the incident angle increases from 0° to 45°. The designed polarization device can also be applied for conformal design due to flexible substrates. The simulation and experiment results have demonstrated that our proposed polarizer can still keep high polarization conversion efficiency even when adhered to convex cylindrical surfaces. The proposed periodical metallic structure has great potential application values in the microwave, terahertz, and optic regimes.

2. Structure design and theoretical analysis

Figure 1 shows the structure of the polarization converter used in the simulations and experiments. The polarizer is composed of four layers with the periodic metallic structure on the top and the metallic ground plane on the bottom separated by two flexible material layers. The 30 μm thick copper film is used as the metallic parts and polyethylene terephthalate (PET) is chosen as the flexible material with a thickness of $d_1 = 0.12$ mm. The relative dielectric constant of PET is 2.86 with a dielectric loss tangent of 0.053. Because the thickness of PET is not enough for the microwave polarizer design, polyvinyl chloride (PVC, $\varepsilon_r = 3 \times (1 - j0.014)$) with a thickness of $d_2 = 2$ mm is filled in the area between the PET layer and the ground plane. The top metallic unit cell is composed of three parts, the long arc metallic wire, the short arc metallic wire, and the metallic disk. As shown in Fig. 2(a), the final geometrical parameters of the unit cell are: $w = 0.4$ mm, $r_1 = r_2 = 2.4$ mm, $r_3 = 1.5$ mm, $\alpha = 190°$, and $\beta = 33°$. The designed polarizer consists of 48×48 square unit cells (5 mm × 5 mm). The top metallic structure can be regarded as an anisotropic metamaterial layer for its asymmetrical structure along the *x*-axis and *y*-axis.

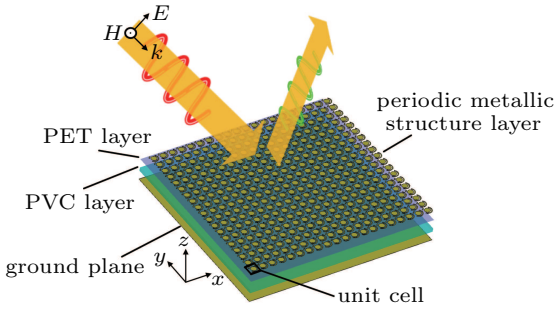


Fig. 1. The structure diagram of the proposed polarization converter.

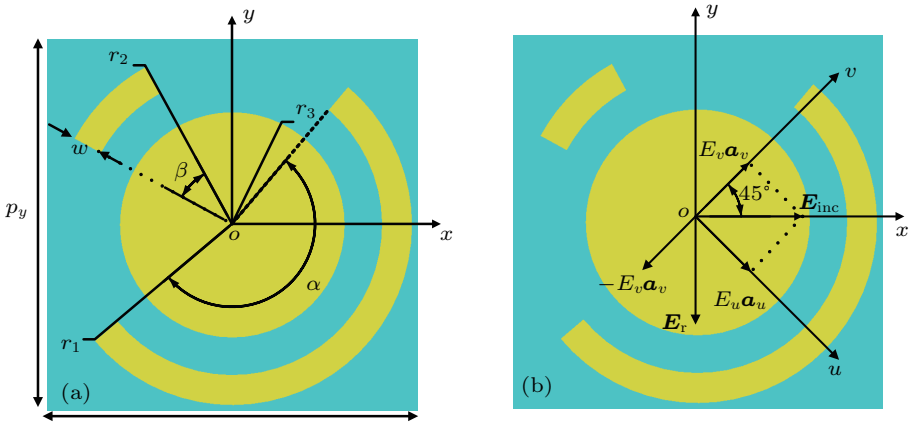


Fig. 2. The unit cell of the metasurface: (a) front view of the unit cell, and (b) intuitive scheme of *x*- to *y*-polarization EM wave conversion of the metasurface.

To illuminate the polarization conversion theory, we assume that an *x*-polarized electromagnetic wave is normally incident on the polarization converter (the same as a *y*-polarized wave). The electronic field of the incident electromagnetic wave denoted as $\boldsymbol{E}_{\rm inc} = E_x \boldsymbol{a}_x$ can be decomposed into the *u*-polarized and *v*-polarized components denoted as $E_u \boldsymbol{a}_u$ and $E_v \boldsymbol{a}_v$, respectively, as shown in Fig. 2(b). In this way, the electric field vector $\boldsymbol{E}$ in the incident wave and the reflected wave can be expressed as Eqs. (1) and (2), respectively

$$\boldsymbol{E}_{\rm inc} = E_x \boldsymbol{a}_x = E_x \cos(45°)(\boldsymbol{a}_u + \boldsymbol{a}_v) = E_u \boldsymbol{a}_u + E_v \boldsymbol{a}_v, \quad (1)$$

$$\boldsymbol{E}_{\rm r} = R \cdot \boldsymbol{E}_{\rm inc} = (\boldsymbol{a}_u \ \ \boldsymbol{a}_v) \begin{pmatrix} r_{uu} & r_{uv} \\ r_{vu} & r_{vv} \end{pmatrix} \begin{pmatrix} E_u \\ E_v \end{pmatrix}, \quad (2)$$

where $\boldsymbol{a}_u$ and $\boldsymbol{a}_v$ are the unit vectors in the *u*-axis and *v*-axis directions, r_{uu} or r_{vv} represents the co-polarization reflection coefficient, and r_{uv} or r_{vu} represents the cross-polarization reflection coefficient, respectively, at the *u*-polarized or *v*-polarized wave incidence. Due to the symmetric structure along the *u*-axis, the amplitudes of r_{uv} and r_{vu} are near to 0, which means that no cross-polarized reflection exists at *u*-polarized and *v*-polarized EM wave incidences. According to these conditions,

equation (2) can be written as

$$\boldsymbol{E}_{\rm r} = E_u r_{uu}\boldsymbol{a}_u + E_v r_{vv}\boldsymbol{a}_v = E_x\cos(45^\circ)(r_{uu}\boldsymbol{a}_u + r_{vv}\boldsymbol{a}_v), \quad (3)$$

where $r_{uu} = |r_{uu}|e^{j\varphi_u}$ and $r_{vv} = |r_{vv}|e^{j\varphi_v}$.

Then, if conditions

$$|r_{uu}| = |r_{vv}| = 1, \quad (4)$$

$$\Delta\varphi = \varphi_u - \varphi_v = \pi + 2n\pi, \quad (5)$$

are satisfied (n is an integer), then

$$\begin{aligned}\boldsymbol{E}_{\rm r} &= E_x\cos(45^\circ)e^{j\varphi_v}(\boldsymbol{a}_u + e^{j\Delta\varphi}\boldsymbol{a}_v)\\ &= E_x\cos(45^\circ)e^{j\varphi_v}(\boldsymbol{a}_u - \boldsymbol{a}_v) = -E_x e^{j\varphi_v}\boldsymbol{a}_y, \end{aligned} \quad (6)$$

the polarization direction of the reflected light is transformed to the y-axis.

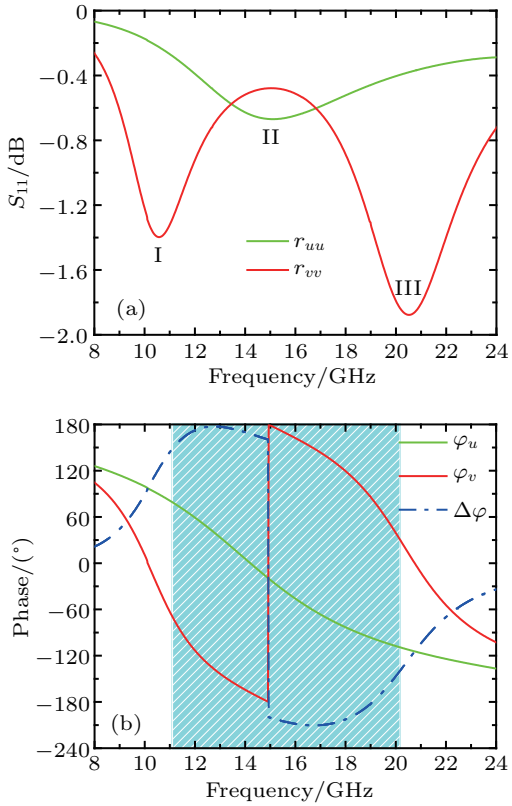


Fig. 3. The co-polarization reflection coefficients for u- and v-axes. (a) Magnitude; (b) phase and phase difference.

Figure 3 presents the simulated magnitudes and phases of r_{uu} and r_{vv} of the optimized polarizer based on Computer Simulation Technology (CST) Microwave Studio. It is clear that the magnitudes of r_{uu} and r_{vv} are close to 1 in Fig. 3(a), and the absolute value of phase difference $\Delta\varphi$ is close to 180° from 11.3 GHz to 20.2 GHz in the blue area in Fig. 3(b). So the conditions in Eqs. (4) and (5) are met, which means that the polarization direction of the reflected wave is rotated by 90° with the proposed polarizer. From the view of resonance,[33] the electric field along the v-axis can excite two magnetic resonances (I and III), and along the u-axis can excite one electric resonance (II). Here, the electric (magnetic) resonance does not necessarily mean out-of-phase (in-phase) reflection in Ref. [27], and the resonance type is judged through surface current distributions at the corresponding resonant frequency. Given the length of this paper, the current distributions at the three resonant frequencies are not presented here. In fact, the unit cell of the designed polarizer is a combined structure and it can excite multiple resonances. Moreover, main resonances are excited by the long arc metallic wire and the metallic disk because the resonance frequency of the short arc wire is out of the designed frequency band.

3. Simulation results

To verify the wideband property of the designed metasurface, full-wave simulations are performed with frequency domain solver in CST Microwave Studio. We set the periodic boundary conditions in x and y directions and open conditions along the z-axis. The polarization conversion ratio (PCR) can be defined as

$$\text{PCR} = r_{yx}^2/(r_{yx}^2 + r_{xx}^2) \quad \text{or} \quad r_{xy}^2/(r_{xy}^2 + r_{yy}^2), \quad (7)$$

where r_{xx} or r_{yy} is the co-polarization reflection coefficient, and r_{yx} or r_{xy} is the cross-polarization coefficient when x-polarized or y-polarized EM wave propagates along the z-axis

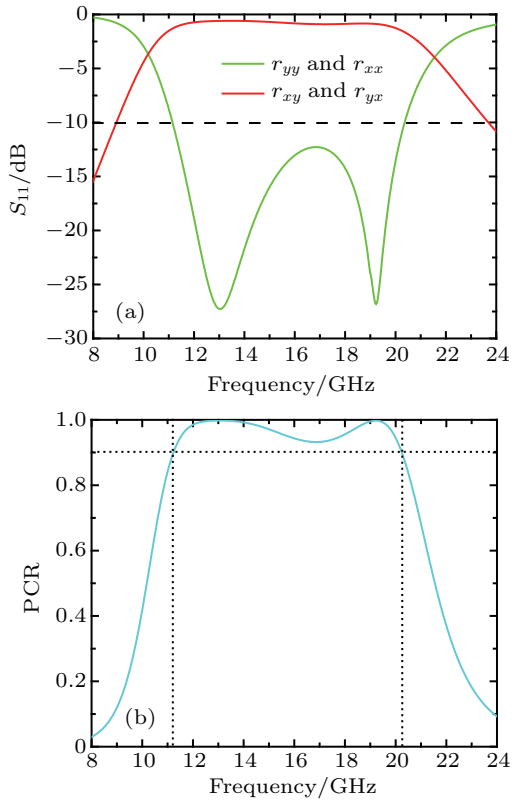


Fig. 4. Under normal incidence, (a) simulated reflection coefficients, (b) PCR with $r_3 = 1.5$ mm.

direction. Because of the symmetric structure along the u-axis, PCR, co-polarization, and cross-polarization reflection coefficients are the same under the normal incidence of x- or y-polarized EM wave. We can find that r_{xy} and r_{yx} are higher than -1 dB, and r_{yy} and r_{xx} are lower than -10 dB in the frequency range from 11.3 GHz to 20.2 GHz in Fig. 4(a). It can also be seen from Fig. 4(a) that there are two resonant frequencies, one at 13.0 GHz and the other at 19.2 GHz. As shown in Fig. 4(b), PCR is higher than 90% from 11.3 GHz to 20.2 GHz under normal incidence. At the two resonant frequencies of 13.0 GHz and 19.2 GHz, the values of PCR are close to 100%. The simulation results demonstrate that the proposed polarizer can achieve wideband linear polarization conversion.

3.1. Impact of metallic disk radius

To investigate the effects of the metallic disk on polarization conversion, we have carried out numerical simulations by changing the radius of the metallic disk. Figure 5(a) indicates that r_3 can have great effects on the resonant frequencies and operating bandwidth under normal incidence of the y-polarized wave (the same as the x-polarized wave). With the increase of the radius of the metallic disk, the bandwidth decreases and the first resonant frequency shows a blue shift while there is a large red shift on the second and third frequencies. When $r_3 = 1.5$ mm, the first two resonant frequencies come into one frequency. The above analysis is also available for the oblique incidence under $\theta = 40°$ as shown in Fig. 5(b), except that there are only two resonant frequencies under oblique incidence even if r_3 varies from 1.1 mm to 1.6 mm. Additionally, we calculate the minimum PCR between the first resonant frequency and the last resonant frequency from the simulated results. As shown in Fig. 6, when the radius of the metallic disk r_3 becomes longer, the minimum PCR gradually decreases under normal incidence, but it gradually rises when r_3 is lower than 1.6 mm under $\theta = 40°$. In particular, the minimum values of PCR are all higher than 90% under both $\theta = 0°$ and $\theta = 40°$ when r_3 is 1.5 mm.

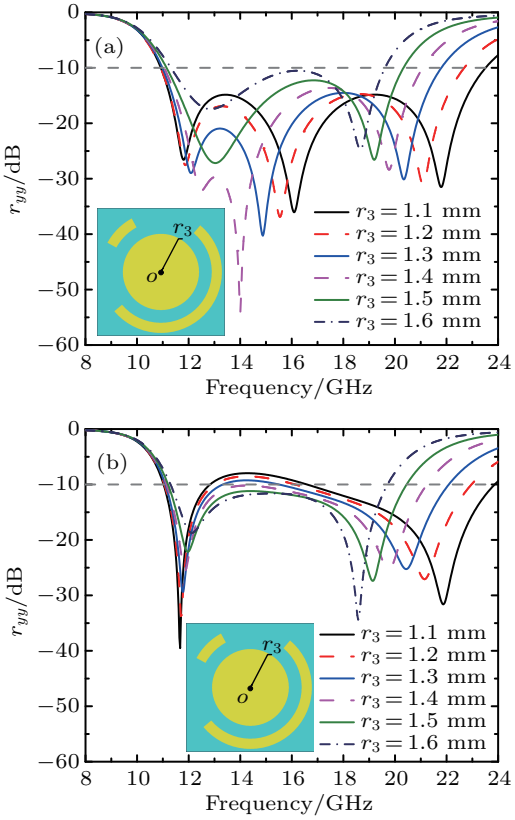


Fig. 5. Simulated co-polarization reflection coefficients with r_3 varying from 1.1 mm to 1.6 mm. (a) Incident angle $\theta = 0°$; (b) $\theta = 40°$.

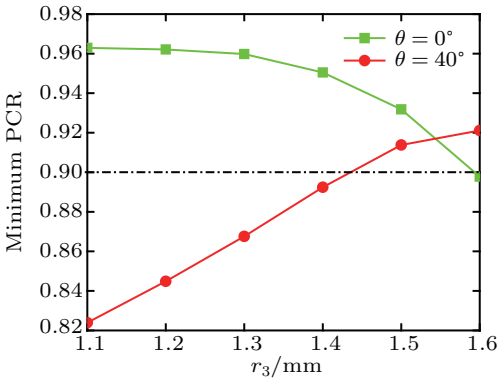


Fig. 6. Simulated minimum PCR between the first resonant frequency and the last resonant frequency with r_3 varying from 1.1 mm to 1.6 mm.

3.2. Incident angle insensitivity analysis

The most important criterion for obtaining a very weak angular dependence is to avoid coupling to propagating first negative diffraction orders, which is related to the unit cell periodicity p of the polarization conversion metasurface according to Bragg's law.[46] In addition, the thickness of the substrate also exerts strong influence on the angle independence.[33] As shown in Fig. 7(a), the electromagnetic waves run back and forth in the dielectric substrates. The reflected coefficient on the boundary between the PET and PVC layer is $\Gamma = (\sqrt{\varepsilon_2} - \sqrt{\varepsilon_1})/(\sqrt{\varepsilon_2} + \sqrt{\varepsilon_1}) = 0.012$, where ε_1 and ε_2 represent the real parts of dielectric constants of the PET and PVC materials, respectively. Due to the thin thickness d_1 of the PET and the small value of Γ, the two layers can be equivalent to one PVC layer with the thickness $d_1 + d_2$ in Fig. 7(b). The additional phase due to the oblique incidence is defined as $\Delta\varphi_{\text{add}}$

$$\begin{aligned}\Delta\varphi_{\text{add}} &= \varphi_{\text{obl}} - \varphi_{\text{nor}} = 2\sqrt{\varepsilon_2}k_0(d_1+d_2)(1/\cos\gamma - 1)\\ &= 2\sqrt{\varepsilon_2}k_0(d_1+d_2)(1/\sqrt{(1-(\sin^2\theta/\varepsilon_2)} - 1), \quad (8)\end{aligned}$$

where φ_{obl} and φ_{nor} are the phases of the incident wave in the dielectric layer under oblique incidence and normal incidence, respectively, γ represents the refraction angle, and k_0 is the wave number in the air. When other parameters are the same, thinner thickness leads to less additional phase, which would be beneficial to keep better polarization conversion ratio under oblique incidence.

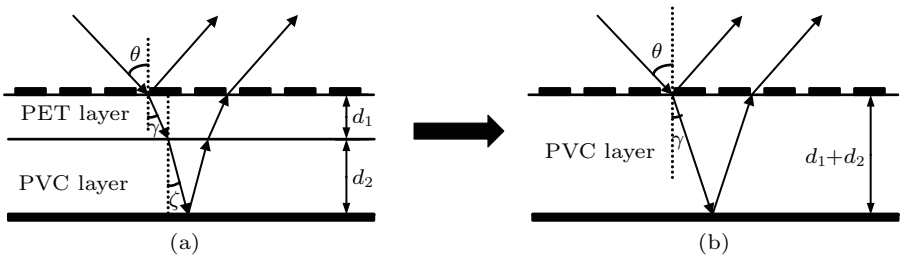


Fig. 7. Schematic diagram of EM wave propagation in (a) two dielectric plates and (b) a dielectric plate for oblique incidence.

Our designed polarizer has optimized the size and thickness of the unit cell; here, we make a comparison with some other reflection linear polarization converters in Table 1. In Table 1, BW indicates the operating absolute bandwidth (PCR $>$ 90%) of the metasurface. The parameters p and t are the unit cell periodicity of the polarization conversion metasurface and the dielectric substrate thickness of the metasurface, respectively. $\Delta\varphi_{\rm add}$(max) is defined as the maximum additional phase under the incident angle of 45° and $\lambda_{\rm min}$ is the wavelength of the incident wave at the lowest operating frequency in the air. The incident angle dependence can be reduced by our designed polarization converter despite the fact that the bandwidth is reduced at the same time.

Table 1. Comparison with other wideband polarization conversion metasurfaces.

	p/mm	t/mm	BW/GHz	$p/\lambda_{\rm min}$	$\Delta\varphi_{\rm add}$(max)
Ref. [29]	12.5	4.0	5.2–12.1	0.504	15.58°
Ref. [32]	10	3	6.84–16	0.533	28.07°
Ref. [33]	6.4	1.6	12.4–27.96	0.596	28.87°
Present study	5	2.12	11.3–20.2	0.338	17.07°

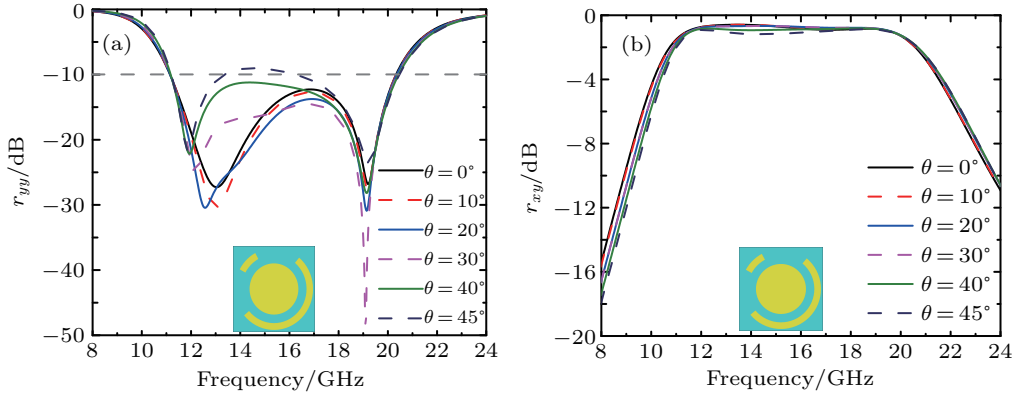


Fig. 8. Simulated (a) co-polarization and (b) cross-polarization reflection coefficients of the proposed polarizer under the oblique incidence of y-polarized electromagnetic waves when θ varies from 0° to 45° ($r_3 = 1.5$ mm).

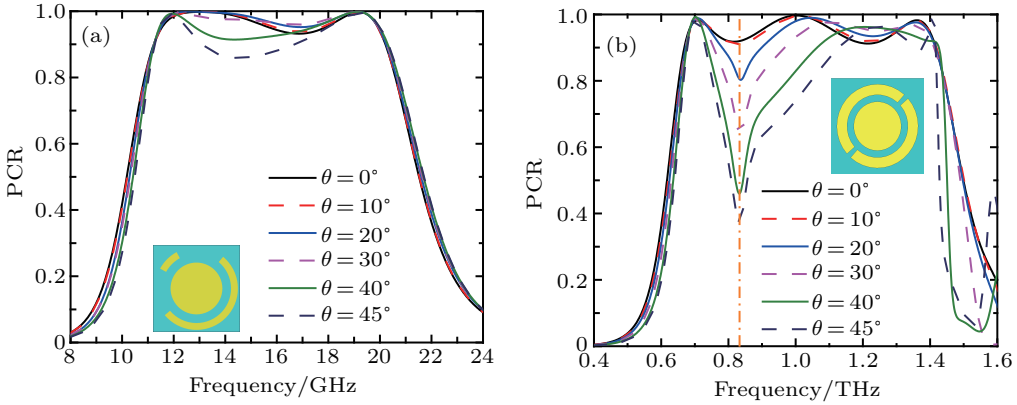


Fig. 9. Simulated PCR of (a) the proposed polarizer and (b) the polarizer based on the DSRRs under the oblique incidence of y-polarized electromagnetic waves with θ from 0° to 45° ($r_3 = 1.5$ mm).

Then, we study the polarization conversion of the optimized structure under the oblique incidence of y-polarized EM waves. Figure 8(a) presents that the first resonance becomes weaker and amplitudes of r_{yy} at the last resonant frequency remain below −20 dB with the increase of θ from 0° to 45°. Meanwhile, figure 8(b) shows that the cross-polarization re-

flection coefficients are not greatly affected by the incident angle from 0° to 45°. The values of PCR are calculated from those simulated co- and cross-polarization reflection coefficients. As can be seen from Fig. 9(a), even if θ is increased to 40° and 45°, the values of PCR can still keep higher than 90% from 11.2 GHz to 20.3 GHz and over 85% from 11.2 GHz to 20.5 GHz, respectively. BW remains nearly unchanged as θ increases from 0° to 45°. The simulated results further demonstrate that our designed polarization converter can work well with a wide range of incident angles. Furthermore, compared with the symmetric structure composed of the split-ring resonators and metallic disk resonators (together hereinafter referred to as DSRRs) in Ref. [31], our proposed asymmetric structure can avoid the split of the bandwidth which is caused by the absorption, as shown in Figs. 9(a) and 9(b).

3.3. Current distributions

From the perspective of resonances, the surface current distributions are given in Fig. 10 at resonant frequencies under $r_3 = 1.4$ mm and $r_3 = 1.5$ mm (different resonant numbers as shown in Fig. 5(a) and similar minimum PCR values in Fig. 6) to explain the physical mechanism of the reflected linear polarization converter. There are three resonances at 12.5 GHz, 14.0 GHz, and 19.8 GHz when $r_3 = 1.4$ mm. The surface current distributions at these resonant frequencies on the top metallic structure and metallic ground sheet are shown in Figs. 10(a)–10(c). The top metallic structure forms an equivalent surface current at 12.5 GHz and 14.0 GHz, which is antiparallel to the current flowing on the bottom ground plane. In this case, an equivalent circulating current is formed between the top metallic structure and the metallic ground, and magnetic resonances are created at those two resonant frequencies. On the contrary, the surface current on the top metallic structure is parallel to the current on the ground plane at 19.8 GHz, which can be regarded as an electric dipole that can excite the electric resonance. Under $r_3 = 1.5$ mm, there is a magnetic resonance at 13.0 GHz and an electric resonance at 19.2 GHz in the same analytical way, as shown in Figs. 10(d) and 10(e).

We can find that the current on the metallic ground sheet at 14.0 GHz in Fig. 10(b) is much weaker than that at other resonant frequencies, which means that the magnetic resonance at 14.0 GHz is easily broken. Moreover, with the increase of the incident angle, the magnitude of the electric field along the u-axis and v-axis (y-polarized wave decomposed into the two directions) would decrease, which would lead to the weaker magnetic resonance. Thus, the second resonant frequency would disappear when the incident angle $\theta = 40°$ as shown in Figs. 5(a) and 5(b).

Furthermore, it can be seen that most of the current distributes on the long arc metallic wire and metallic disk and a little on the short arc metallic wire, which confirms long arc metallic wire and metallic disk make greater contributions to resonances.

It is also necessary to point out that the y-polarized wave (the same as the x-polarized wave) could excite all the three resonant modes (I), (II), and (III) in Fig. 3(a) because the electric field of it can be decomposed into two components along the u-axis and v-axis, respectively. These resonant modes would generate resonance frequencies of different positions and numbers through mutual coupling.

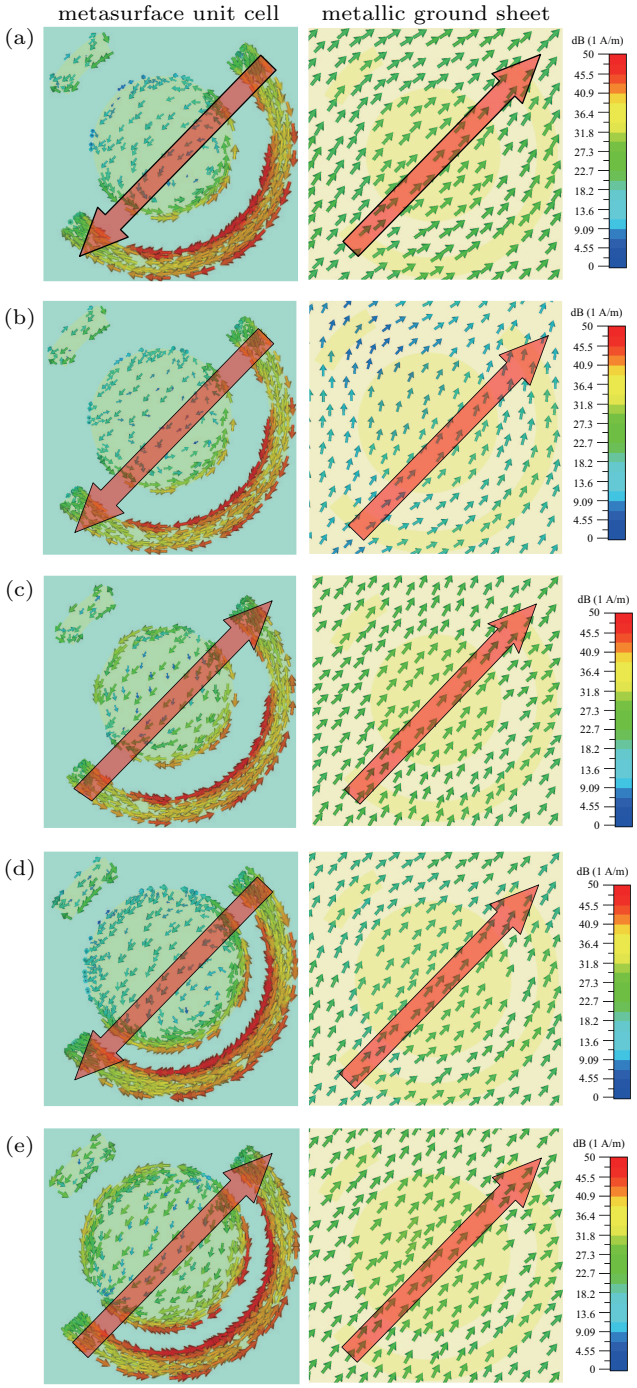


Fig. 10. The current distributions on the metasurface (left column) and metallic ground sheet (right column) under y-polarized wave incidence when $r_3 = 1.4$ mm at (a) 12.5 GHz, (b) 14.0 GHz, (c) 19.8 GHz, and when $r_3 = 1.5$ mm at (d) 13.0 GHz, (e) 19.2 GHz. The red arrow indicates the equivalent current direction.

3.4. Conformal performance

To study the conformal performance, the designed polarizer and the pure metallic sheet are bent on convex cylindrical surfaces respectively with different curvature radii $R =$ 250 mm and $R = 500$ mm, as shown in Figs. 11(a), 11(b) and 11(c), 11(d). We define σ_{yy} as the co-polarization radar cross section (RCS) and σ_{xy} as the cross-polarization RCS under the y-polarized plane wave

$$\sigma_{yy} = 4\pi D^2 |\boldsymbol{E}_y^{\mathrm{r}}|^2 / |\boldsymbol{E}_y^{\mathrm{i}}|^2, \quad \sigma_{xy} = 4\pi D^2 |\boldsymbol{E}_x^{\mathrm{r}}|^2 / |\boldsymbol{E}_y^{\mathrm{i}}|^2, \tag{9}$$

where D is the distance from the metasurfaces to the observation points, $\boldsymbol{E}^{\mathrm{r}}$ and $\boldsymbol{E}^{\mathrm{i}}$ are the scattered and incident electric fields, respectively, and $\boldsymbol{E}_x$ and $\boldsymbol{E}_y$ are electric fields along the x-axis and y-axis, respectively. RCS can be used to analyze the polarization conversion of our designed polarizer on curved surfaces with the same D based on Eq. (9). Figures 11(a), 11(c) and 11(b), 11(d) show the simulated 3D bistatic RCS including co-polarization RCS σ_{yy} and cross-polarization RCS σ_{xy} under normal incidence of y-polarized EM wave with our designed polarizer and the same shaped metal cylindrical metallic sheets, respectively. For metallic curved sheet, main scattered energy distributes in the co-polarization component and little in the cross-polarization component, as can be seen in Figs. 11(b) and 11(d). In contrast, cross-polarization RCS is much higher than co-polarization RCS in the main scattered area for our designed polarizer under $R = 250$ mm and $R = 500$ mm in Figs. 11(a) and 11(c), which indicates that our proposed polarizer conformal on the curved surface can achieve polarization conversion. Besides, in the column titled with cross-polarization of Figs. 11(a) and 11(c), when R increases from 250 mm to 500 mm, the energy of the scattered wave propagating along the $+z$-axis would increase and the beamwidth of the lobe along the $+z$-axis in the xoz plane would be narrower, which indicates that the energy of the scattered wave would be more concentrated.

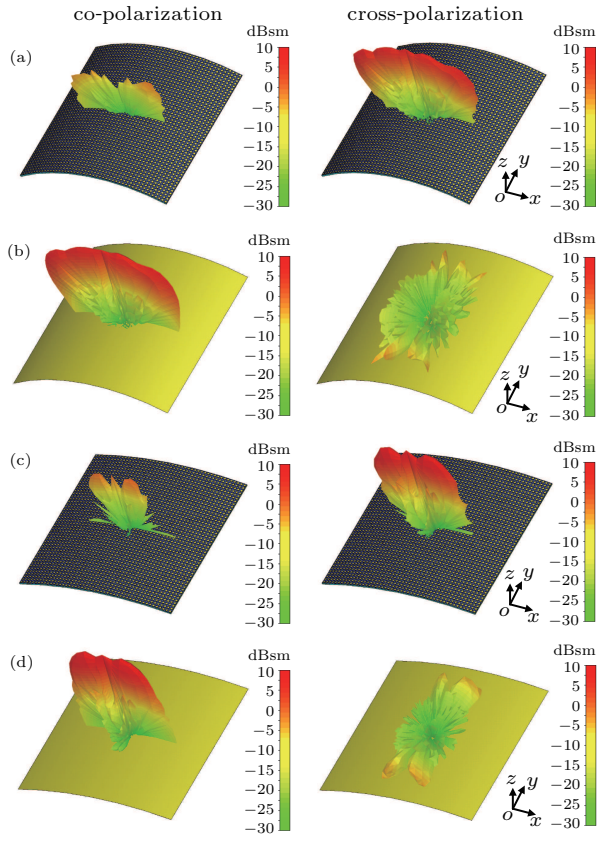


Fig. 11. Bi-static 3D σ_{yy} and σ_{xy} of the polarizer on the (a) and (c) convex cylindrical surface, and (b) and (d) metal convex cylindrical surface, with different curvature radii (a) and (b) $R = 250$ mm and (c) and (d) $R = 500$ mm at 13.0 GHz.

4. Experiments

To experimentally show properties of the proposed polarization converter, some prototypes are fabricated on PET substrate and stuck on the PVC substrate with these parameters $d_1 = 0.12$ mm, $d_2 = 2$ mm, $w = 0.4$ mm, $r_1 = r_2 = 2.4$ mm, $r_3 = 1.5$ mm, $\alpha = 190°$, and $\beta = 33°$. Figure 12 shows the photo of the fabricated prototype and the measurement setup. The sample is placed in the front of the horn antennas surrounding by absorbing materials, and the horn antennas are fixed on the two vertical arms of the rotating pedestal. The centers of the sample and horn antennas are set at the same height. One horn antenna is used as the source and the other is used for receiving reflected waves to obtain the co- and cross-polarization reflective coefficients by rotating the receiving antenna by 0° and 90°. Both antennas are connected to an Agilent vector network analyzer (N5245A). The horizontal arms connected to the rotating pedestal can be rotated to obtain the reflective coefficients under different incident angles. However, the separation angle between the two antennas is set to be 5° firstly because of their overlap positions under normal incidence. It should be noted that the metal ground sheet is also measured for the sake of normalization.

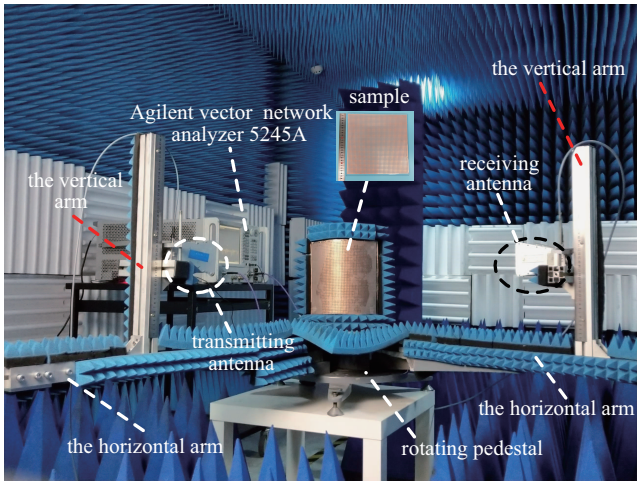


Fig. 12. Fabricated metasurfaces with parameters: $d_1 = 0.12$ mm, $d_2 = 2$ mm, $w = 0.4$ mm, $r_1 = r_2 = 2.4$ mm, $r_3 = 1.5$ mm, $\alpha = 190°$, and $\beta = 33°$, and experimental setup.

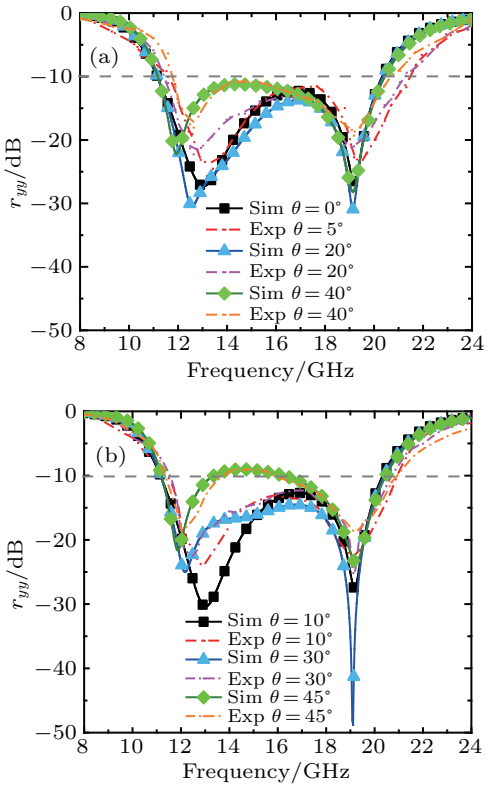


Fig. 13. The simulated and measured magnitude of r_{yy} (a) with $\theta = 0°$, 20°, and 40°; (b) with $\theta = 10°$, 30°, and 45°.

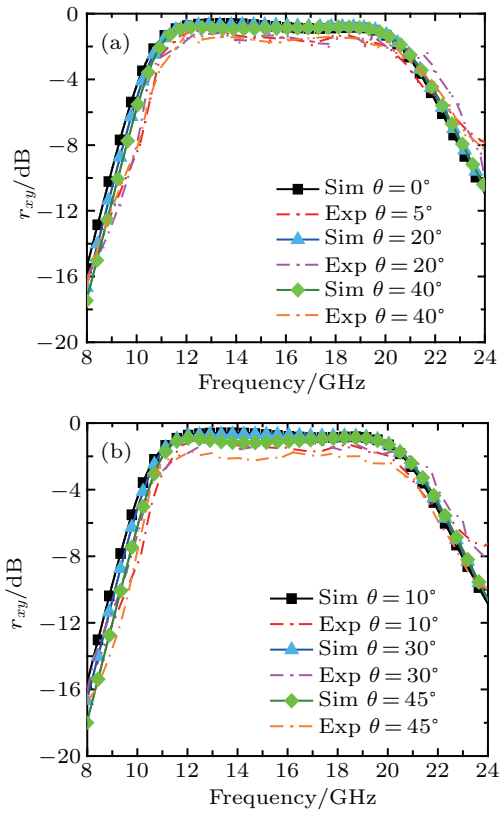


Fig. 14. The simulated and measured magnitude of r_{xy} (a) with $\theta = 0°$, 20°, and 40°; (b) with $\theta = 10°$, 30°, and 45°.

Figures 13 and 14 illustrate the simulated and measured reflective coefficients, which indicate that the experiment results are in good agreement with numerical predictions. We can clearly observe two resonant frequencies when the incident angle varies from 5° to 45°. PCR is also given in Fig. 15(a), which is in good agreement with the simulation. Moreover, in order to show the conformal feature of our proposed polarizer, some arc foams have been made and the sample is stuck on the different convex cylindrical surfaces of them and tested. Limited by the testing condition, the measured bistatic RCS cannot be obtained at present and we use *S*-parameters to evaluate the polarization conversion. The same cylindrical metal ground sheets are measured for the sake of normalization without taking influences of scattering waves brought by the cylindrical structure into consideration. Figure 15(b) shows the calculated PCR from the measured results. The designed polarization converter can keep high polarization conversion efficiency from 11.9 GHz to 20.0 GHz even it is bent on convex cylindrical surfaces.

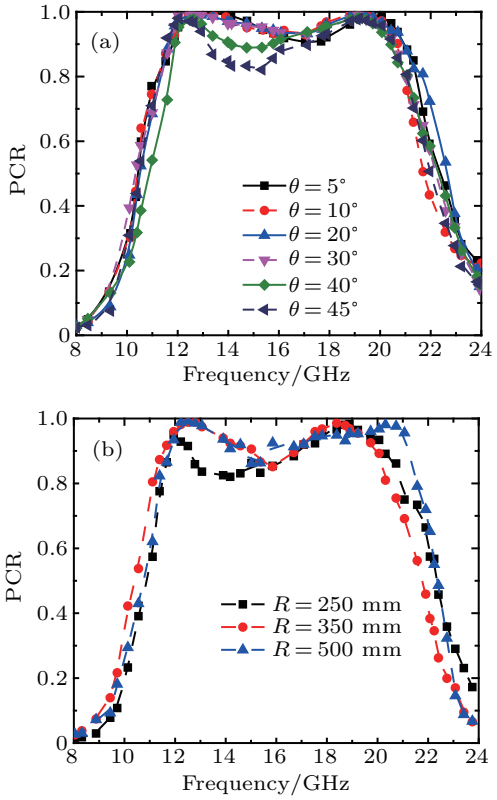


Fig. 15. (a) The experimental PCR with θ varying from 5° to 45° when the sample is placed on the plane. (b) The experiment PCR when the sample is stuck on the convex cylindrical surface with R varying from 250 mm to 500 mm.

5. Conclusion

In this paper, we have proposed a high-efficient, broadband, and wide-angle reflective polarization converter based on flexible metasurface at microwave band. The operation bandwidth has been expanded greatly because of the presence of these resonances. The physics mechanism is illustrated by simulating the reflected amplitudes and phase differences between *u*- and *v*-polarized incident EM waves. Due to the combination of the first two resonances into one and the optimized

size and thickness of the unit cell, the polarization converter can keep high-efficient polarization conversion over a broadband frequency range when the angle of incident electromagnetic waves varies from 0° to 45°. The surface current distributions at resonant frequencies are also given to further analyze the physical mechanism of the polarizer. Both the simulation and the experimental results have shown that the values of PCR can keep over 90% from 11.2 GHz to 20.3 GHz when the incidence angle changes from 0° to 40°. Additionally, the sample stuck on convex cylindrical surfaces with different curvature radii R is tested, and the tested results show good polarization conversion and flexibility of our designed polarizer. Compared with previous research, this can not only have wide bandwidth, high efficiency, and a weak angular dependence but can also be conformal with the surfaces of the automobiles, airplanes, steamships, and so on. The designed structure has great potential application values in the microwave, terahertz, and optic regimes.

References

[1] Dietlein C, Luukanen A, Popović Z and Grossman E 2007 *IEEE Trans. Antennas Propag.* **55** 1804
[2] Chattopadhyay T, Bhowmik P and Roy J N 2012 *J. Opt. Soc. Am. B* **29** 2852
[3] Shelby R A, Smith D R and Schultz S 2001 *Science* **292** 77
[4] Shelby R A, Smith D R, Nemat-Nasser S C and Schultz S 2001 *Appl. Phys. Lett.* **78** 489
[5] Huang X J, Yang D and Yang H L 2014 *J. Appl. Phys.* **115** 103505
[6] Ma H F, Wang G Z, Kong G S and Cui T J 2014 *Opt. Mater. Express* **4** 1717
[7] Cheng Y Z, Nie Y, Cheng Z Z, Wu L, Wang X and Gong R Z 2013 *J. Electromagn. Waves Appl.* **27** 1850
[8] Kundtz N and Smith D R 2010 *Nat. Mater.* **9** 129
[9] Yu N F and Capasso F 2014 *Nat. Mater.* **13** 139
[10] Liu K, Liu Y, Jia Y T and Guo Y J 2017 *IEEE Trans. Antennas Propag.* **65** 4288
[11] Jia Y T, Liu Y, Gong S X, Zhang W B and Liao G S 2017 *IEEE Antennas Wireless Propag. Lett.* **16** 2477
[12] Ni X J, Wong Z J, Mrejen M, Wang Y and Zhang X 2015 *Science* **349** 1310
[13] Bückmann T, Thiel M, Kadic M, Schittny R and Wegener M 2014 *Nat. Commun.* **5** 4130
[14] Meissner T and Wentz F J 2006 *IEEE Trans. Geosci. Remote Sens.* **44** 506
[15] Hao J M, Yuan Y, Ran L X, Jiang T, Kong J A, Chan C T and Zhou L 2007 *Phys. Rev. Lett.* **99** 063908
[16] Ma X L, Huang C, Pu M B, Hu C G, Feng Q and Luo X G 2012 *Opt. Express* **20** 16050
[17] Winkler S A, Hong W, Bozzi M and Wu K 2010 *IEEE Trans. Antennas Propag.* **58** 1202
[18] Cheng Y Z, Nie Y, Cheng Z Z and Gong R Z 2014 *Prog. Electromagn. Res.* **145** 263
[19] Song K, Liu Y H, Luo C R and Zhao X P 2014 *J. Phys. D: Appl. Phys.* **47** 505104
[20] Wu L, Yang Z Y, Cheng Y Z, Gong R Z, Zhao M, Zheng Y, Duan J A and Yuan X H 2014 *Appl. Phys. A* **116** 643
[21] Wei Z Y, Cao Y, Fan Y C, Yu X and Li H Q 2011 *Appl. Phys. Lett.* **99** 221907
[22] Li Y F, Zhang J Q, Qu S B, Wang J F, Zheng L, Pang Y Q, Xu Z and Zhang A X 2015 *J. Appl. Phys.* **117** 044501
[23] Jia Y T, Liu Y, Zhang W B and Gong S X 2016 *Appl. Phys. Lett.* **109** 051901
[24] Yogesh N, Fu T, Lan F and Ouyang Z B 2015 *IEEE Photon. J.* **7** 1
[25] Gansel J K, Thiel M, Rill M S, Decker M, Bade K, Saile V, Freymann G V, Linden S and Wegener M 2009 *Science* **325** 1513
[26] Feng M D, Wang J F, Ma H, Mo W D, Ye H J and Qu S B 2013 *J. Appl. Phys.* **114** 074508
[27] Chen H Y, Wang J F, Ma H, Qu S B, Xu Z, Zhang A X, Yan M B and Li Y F 2014 *J. Appl. Phys.* **115** 154504
[28] Wu J L, Lin B Q and Da X Y 2016 *Chin. Phys. B* **25** 088101
[29] Dong G X, Shi H Y, Xia S, Zhang A X, Xu Z and Wei X Y 2016 *Opt. Commun.* **365** 108
[30] Jiang Y N, Wang L, Wang J, Akwuruoha C N and Cao W P 2017 *Opt. Express* **25** 27616
[31] Cheng Y Z, Withayachumnankul W, Upadhyay A, Headland D, Nie Y, Gong R Z, Bhaskaran M, Sriram S and Abbott D 2014 *Appl. Phys. Lett.* **105** 181111
[32] Mei Z L, Ma X M, Lu C and Zhao Y D 2017 *AIP Adv.* **7** 125323
[33] Gao X, Han X, Cao W P, Li H O, Ma H F and Cui T J 2015 *IEEE Trans. Antennas Propag.* **63** 3522
[34] Chen H Y, Wang J F, Ma H, Qu S B, Zhang J Q, Xu Z and Zhang A X 2015 *Chin. Phys. B* **24** 014201
[35] Dong G X, Shi H Y, Xia S, Li W, Zhang A X, Xu Z and Wei X Y 2016 *Chin. Phys. B* **25** 084202
[36] Kim H K, Ling K Y, Kim K and Lim S 2015 *Opt. Express* **23** 5898
[37] Wang L L, Liu S B, Zhang H F, Kong X K and Liu L L 2017 *J. Electromagn. Waves Appl.* **31** 1216
[38] Sharma S K, Ghosh S, Srivastava K V and Shukla A 2017 *Microwave Opt. Technol. Lett.* **59** 348
[39] Kamali S M, Arbabi A, Arbabi E, Horie Y and Faraon A 2016 *Nat. Commun.* **7** 11618
[40] Jiang Z H, Yun S, Toor F, Werner D H and Mayer T S 2011 *ACS Nano* **5** 4641
[41] Jang Y, Yoo M and Lim S 2013 *Opt. Express* **21** 24163
[42] Xu H X, Tang S W, Sun C, Li L L, Liu H W, Yang X M, Yuan F and Sun Y M 2018 *Photon. Res.* **6** 782
[43] Wu K D, Coquet P, Wang Q J and Genevet P 2018 *Nat. Commun.* **9** 3494
[44] Zhu H, Liang X L, Ye S, Jin R H and Geng J P 2016 *IEEE Antennas Wireless Propag. Lett.* **15** 1653
[45] Jang T, Youn H, Shin Y J and Guo L J 2014 *ACS Photon.* **1** 279
[46] Diem M, Koschny T and Soukoulis C M 2009 *Phys. Rev. B* **79** 033101